MICROCHANNEL FLUID BEHAVIOR USING MICROPOLAR FLUID THEORY

I. Papautsky[1], J. Brazzle[2], T. A. Ameel[3], and A. B. Frazier[1,2]
Departments of [1]Bioengineering, [2]Electrical Engineering, and [3]Mechanical Engineering
University of Utah, Salt Lake City, UT 84112
Tel: (801) 585-9674 Fax: (801) 585-5361 E-mail: ian.papautsky@m.cc.utah.edu

ABSTRACT

In this paper, we describe microchannel fluid behavior using a numerical model based on micropolar fluid theory and experimentally verify the model using micromachined channels. The micropolar fluid theory augments the laws of classical continuum mechanics by incorporating the effects of fluid molecules on the continuum. The behavior of fluids was studied using surface micromachined rectangular metallic pipette arrays. A downstream port for static pressure measurement was used to eliminate entrance effects. The numerical model of the micropolar fluid theory compares favorably with the experimental data.

INTRODUCTION

Research on microfluidic devices fabricated using micromachining technology originated about 20 years ago. A gas chromatograph was developed at Stanford University [1], while ink jet printer nozzles were designed at IBM [2]. With recent improvement of microchannel fabrication methods [3] and the increasing number of fluidic devices with complex microstructures, a whole class of low Reynolds number flows needs to be examined on the microscale. Examples include flows in Micro-Electro-Mechanical Systems (MEMS) fabricated on silicon substrates.

Today, fluid flows in microfabricated fluid systems (i.e. pumps, valves, microchannels) are analyzed using the Navier-Stokes equations [4,5]. However, a number of publications indicate that (a) flows on the microscale are different from that of the macroscale and that (b) Navier-Stokes equations are incapable of explaining the occurring phenomena [6,7]. In addition, experiments show that fluid viscosity close to the channel wall is higher (50 to 80%) than the bulk viscosity of the fluid [8,9]. Thus, the laws of hydrodynamic flow developed for a macroscale continuum fluid (i.e. Navier-Stokes Theory) may no longer be applicable to microscale flow.

Current and future developments of micro fluidic devices, such as pumps, valves, and reactant delivery and separation systems, require the capability to predict expected pressure drops through the fluid-carrying components. The currently available experimental data for micro tubes and channels with characteristic dimension of one to 10's of micrometers is inconclusive. Earlier studies by Wu and Little have indicated a significant (three to five times) increase in friction factor [10]. However, later investigations have demonstrated the exact opposite—a decrease in friction factor on the order of 10% to 20% when compared to macroscale tubes at dynamically similar conditions [11,12]. The most recent studies, however, demonstrate an increase in the friction factor by approximately 50% [5,13]. Some of the possible explanations for this apparent microscale effect include a change in fluid bulk viscosity, consideration of micropolar fluid effects, and slip flow at the solid boundary.

THEORY

The formulation of a general theory of fluid microcontinua is attributed to Eringen [14]. The basis of Eringen's development of "simple microfluids" were his papers with Suhubi [15]. Although their work was concerned with a nonlinear theory of microelastic solids, their treatment of motion, balance of moments, conservation of energy, and entropy production is applicable to all continuous media composed of microelements. Eringen and Suhubi developed a physical model in which each continuum particle is assigned a substructure, i.e. each material volume element contains microvolume elements that can translate, rotate, and deform independently of the motion of the macrovolume. Each deformation of the macrovolume element, however, is expected to produce a subsequent deformation of the microvolume elements. Thus, a mechanism is provided in the theory to treat materials that are capable of supporting local stress moments and body moments and are influenced by the microelement spin inertia.

By definition, a "simple microfluid" is a fluent medium whose properties and behavior are effected by the local motions of the material particles contained in each of its volume elements. Such fluid possesses local inertia. Eringen's simple microfluids are isotropic, viscous fluids and in the simplest case of a linear theory, these

0-7803-4412-X/98/$10.00 © 1998 IEEE

fluids are characterized by 22 viscosity coefficients [14]. However, even for the linear theory, a problem is formulated in terms of a system of nineteen partial differential equations with nineteen unknowns, and the underlying mathematical problem is not easily solvable. This led to consideration of subclasses of the general microfluids that are more amiable to solution and still allow description of the effects arising from particle micromotions.

In micropolar fluids, rigid particles contained in a small volume element can rotate about the center of the volume element described by the micro-rotation vector. This local rotation of the particles is in addition to the usual rigid body motion of the entire volume element. In micropolar fluid theory, the laws of classical continuum mechanics are augmented with additional equations that account for conservation of microinertia moments and balance of first stress moments that arise due to consideration of the microstructure in a material [16]. Thus, new kinematic variables, e.g. the gyration tensor and microinertia moment tensor, and the concepts of body moments, stress moments, and microstress are combined with classical continuum mechanics.

The field equations of the micropolar fluid theory are as follows:

$$\frac{\partial \rho}{\partial t} + \nabla \cdot (\rho \mathbf{V}) = 0 \tag{1}$$

$$(\lambda + 2\mu + \kappa)\nabla\nabla \cdot \mathbf{V} - (\mu + \kappa)\nabla \times \nabla \times \mathbf{V} + \kappa \nabla \times \mathbf{G} - \nabla p + \rho \mathbf{f} = \rho \dot{\mathbf{V}} \tag{2}$$

$$(\alpha + \beta + \gamma)\nabla\nabla \cdot \mathbf{G} - \gamma \nabla \times \nabla \times \mathbf{G} + \kappa \nabla \times \mathbf{V} - 2\kappa \mathbf{G} + \rho \mathbf{l} = \rho j \dot{\mathbf{G}} \tag{3}$$

where a superimposed dot indicates a material derivative and

ρ	= density,
V	= velocity vector,
G	= micro-rotation (gyration) vector,
j	= microinertia,
f	= body force per unit mass vector,
l	= body couple per unit mass vector,
p	= thermodynamic pressure,
μ	= classical shear viscosity coefficient,
λ	= second order viscosity coefficient,
κ	= vortex viscosity coefficient,
α, β, γ	= spin gradient viscosity coefficients.

Equation 1 represents conservation of mass; Equation 2 represents conservation of linear momentum; and Equation 3 represents conservation of micro-inertia. Note that for $\kappa = \alpha = \beta = \gamma = 0$ and vanishing l, gyration G becomes zero and the second equation reduces to the Navier-Stokes equations. Also note that for $\kappa = 0$, the velocity V and the micro-rotation are uncoupled and the global motion is unaffected by the micro-rotations.

For the case of a Newtonian fluid with constant physical properties (water), negligible external forces (no effects of body forces or body couples), and steady-state flow, the equations simplify to

$$\nabla \mathbf{V} = 0 \tag{4}$$

$$(\mu + \kappa)\nabla^2 \mathbf{V} + \kappa \nabla \times \mathbf{G} - \nabla p = 0 \tag{5}$$

$$(\alpha + \beta + \gamma)\nabla^2 \mathbf{G} + \kappa \nabla \times \mathbf{V} - 2\kappa \mathbf{G} = 0 \tag{6}$$

Typically, it is assumed that fluid viscosity is independent of the dimension of the flow channel. A number of studies, however, indicate that for liquids such as water, silicon oil and alcohol this is not a valid assumption. Experimental observations have shown that the viscosity of fluids near a rigid surface (5000 Å or less) is altered significantly as compared to the bulk viscosity measured away from walls [8]. A recent publication [9] indicates that the flow of these thin liquid films may be modeled as flow of Newtonian liquid with an apparent viscosity 50 to 80% higher than that of the bulk. The increase above bulk viscosity is believed to be due either to collective molecular motion effects or to the immobility of the layer of molecules in contact with the solid surface [9]. In addition, experiments with fluids containing extremely small amount of polymeric additives (such as DNA samples for PCR or electrophoresis) indicate that the skin friction near a rigid body in such fluids is considerably lower (up to 35%) than the same fluids without additives [16].

As previously discussed, when the external characteristic length (e.g., film thickness, channel depth) becomes comparable with the internal characteristic length (e.g., molecular dimension, radius of gyration of a polymeric molecule, gas mean free path), the classical Navier-Stokes theory cannot explain the flow behavior. At this stage, the long-range intermolecular forces and molecular packing effects must be taken into account.

Consequently, Eringen and Okada introduced a lubrication theory for fluids with microstructure [17]. This theory presents the following equation for viscosity:

$$\mu = \mu_0 \left[1 + \gamma \left(\frac{R_g}{D} \right)^2 \right] \tag{7}$$

where μ_0 is the bulk viscosity disregarding the inner structure of the fluid, γ is a non-dimensional constant, R_g is the radius of gyration of fluid molecules, and D is an external characteristic length (e.g., the film thickness, channel depth) [17]. The theory produces an excellent

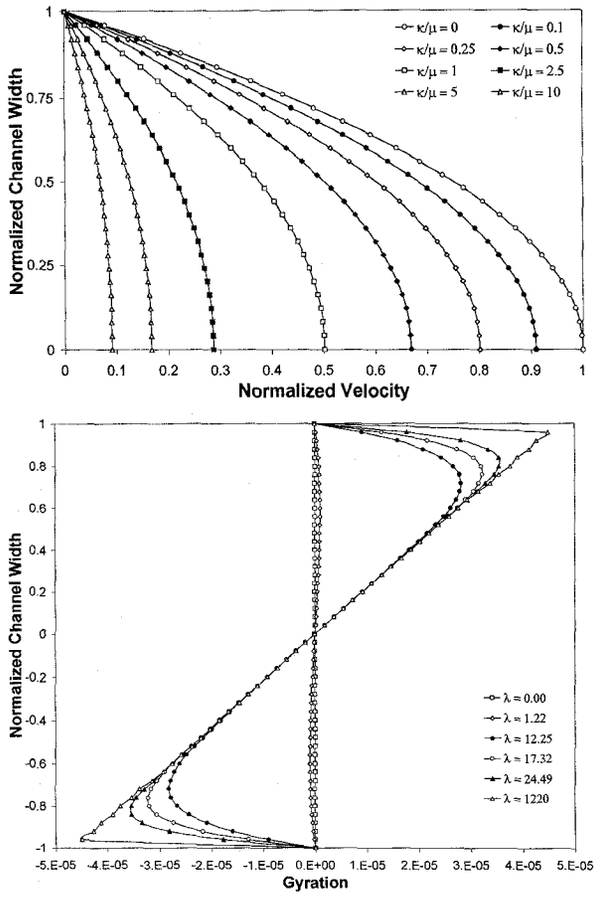

Figure 1. Normalized velocity and micro-rotational velocity (gyration) profiles at the channel centerline.

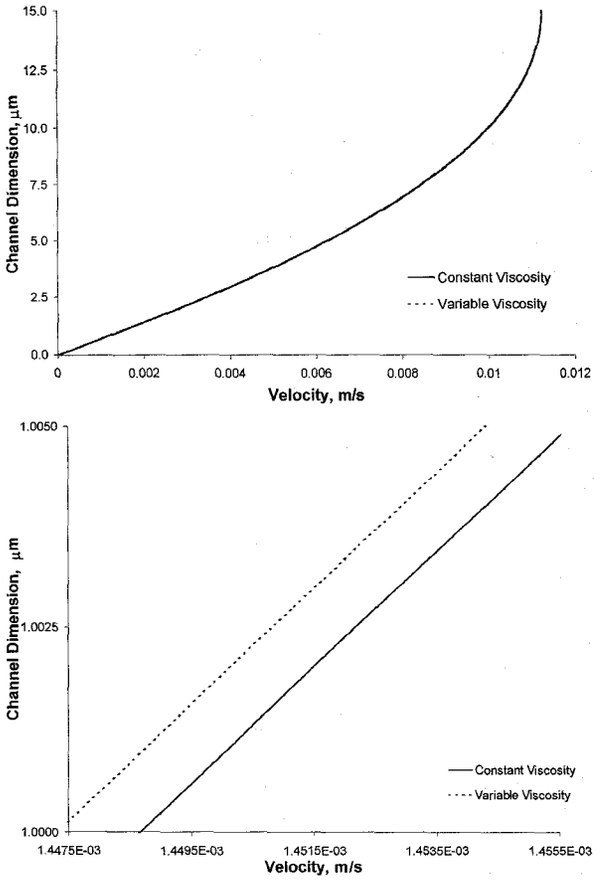

Figure 2. Velocity profiles with fluid viscosity constant and increasing at the side-wall. Note that velocity profiles on the top graph overlap.

fit for data collected by other researchers for film thickness of up to 300 nm. In addition, it is capable of predicting viscosity changes with addition of trace amounts of water to some organic polymers [17].

Equations 5 and 6 have been solved numerically in two dimensions using the finite difference method, with a successive relaxation solution technique, for fluid flow in shallow microchannels. The simulated channel width was 30 μm divided into 300 equal elements. This number was chosen to allow for sufficiently small divisions at the side-walls. An incompressible fluid in a rectangular microchannel was considered as this case represents the conditions expected in many of the proposed fluidic systems. The pressure drop per unit length was set to 100 kPa/m. The channel dimension was defined from the centerline and was normalized by one-half the channel width. The velocity was normalized using the maximum velocity from the Navier-Stokes solution. The numerical model was verified by setting $\kappa = 0$ and comparing results to the Navier-Stokes solution. The ratio of the vortex viscosity coefficient to the shear viscosity coefficient κ/μ is shown to control the velocity profile in the microchannel (Figure 1, top). An additional coefficient λ, which is a combination of vortex and spin gradient viscosity coefficients, is shown to control the micro-rotational velocity (gyration), as shown in Figure 1, bottom. This coefficient is zero when κ is zero, indicating absence of gyration from the Navier-Stokes theory. As the number increases, the micro-rotational effects become more severe, especially at the walls. For blood, the model predicts an 8% reduction in volumetric flow rate compared to the flow rate predicted by the Navier-Stokes equations alone.

The effects of viscosity variation at a channel side-wall were studied by specifying a viscosity vector for the numerical model. In order to separate the effects of viscosity from gyration, κ was set to zero, thus uncoupling Equation 5 from Equation 6. The simulated channel width was 30 μm with dimensions defined from the lower side-wall and pressure per unit length set to 100 kPa/m. While viscosity approaches infinity at the channel wall in theory, the viscosity of water was only increased 3.5 times. At 3000 Å, the viscosity returned to the bulk value of 0.001 N·sec/m^2. The resulting velocity profile is shown in Figure 2, top. In order to see the effects of viscosity more readily, the results are

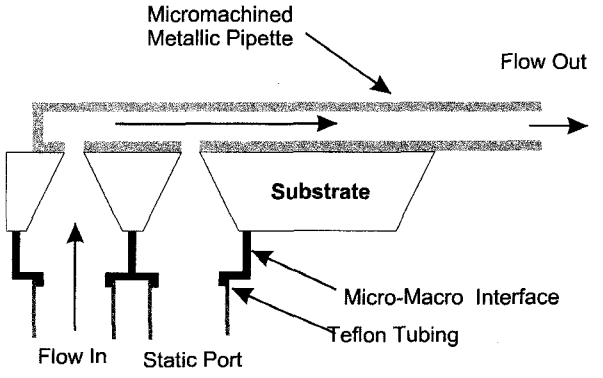

Figure 3. Cross-section schematic diagram of the micromachined pipette input ports and interface for flow experiments.

given in dimensional form. While the change in viscosity resulted only in a very small decrease in the fluid velocity (Figure 2, bottom), the changes were evident up to 8 μm from the side-wall. Overall, the decrease in volumetric flow rate was determined to be less than 0.05% and was therefore not included in the general model.

METHODS

Experiments have been conducted in metallic microchannels using water. Arrays of 5 or 7 metallic microchannels are fabricated using surface micromachining fabrication techniques similar to those previously reported [18,19]. Sections of microchannels that are extended from a silicon substrate are fabricated on top of 5 μm p^+ silicon sacrificial membranes created by KOH etching. The bottom wall is formed by micro electroforming nickel. Thick photoresist is deposited and patterned on top of nickel. The thick photoresist is used to precisely define the inner dimensions of microchannels and serves as a sacrificial layer removed later in the process. The top and side walls are formed by electroforming nickel over a sputtered seed layer. Once the walls are formed, the thick photoresist is removed from the micropipette interior in an acetone bath. Dry etching using SF_6 is used to remove the sacrificial membrane and release the microstructures.

Access ports are fabricated by etching through the substrate for backside access. A cross-section schematic of the micromachined pipette input ports and interface is shown in Figure 3. The use of bottom input ports allowed the macroscale interface between microchannels and macro-tubing to be moved from the front of the device to the back, resulting in a more robust interconnect. The interface provided inputs for fluid flow and downstream ports for static pressure measurement. For the range of experimental flow rates, the entrance length of the developing flow was

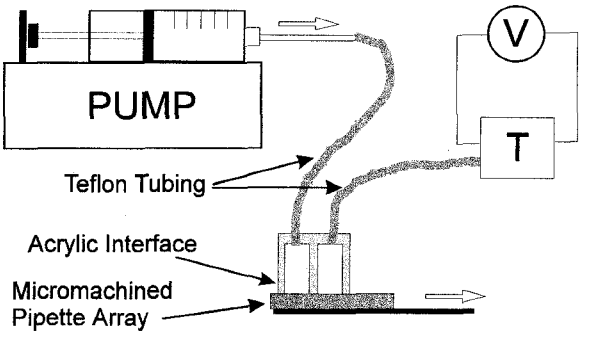

Figure 4. Schematic drawing of the experimental setup (V = voltmeter and T = pressure transducer).

calculated to be less than 0.5 mm. However, the static pressure measurement port was positioned 4 mm downstream in order to eliminate any entrance effects. The extended ends of the pipettes were used as outputs.

Each array consisted of 5 or 7 pipettes. While each pipette had an individual input port, the acrylic interface provided a single pressure source through a manifold. The volume of the manifold was many times greater than the volume of each pipette, allowing a uniform pressure distribution across input ports of the entire array. Thus, the flow through each pipette was assumed to be equal.

Data was collected using the apparatus shown in Figure 4. A controllable syringe pump produced the water flow that was directed to the interface through Teflon tubing. Teflon tubing was also used to connect the static pressure port with a differential pressure transducer T (Omega, PX180-015GV). A digital voltmeter (V) provided the readout of pressure registered by the transducer. Prior to each experiment, tubing connecting the interface and transducer was bled in order to eliminate any air bubbles. During a run, a water droplet would form at the end of the micromachined pipette array. The droplet surface tension increases the outlet pressure above ambient; however, this increase was found to be negligible (< 1%).

RESULTS

Arrays of pipettes of different dimensions have been fabricated on top of silicon substrates for fluid flow studies. The pipettes were 7 mm in length with 2 mm extending from the substrate, while 3 mm separated the pressure ports from the pipette ends. The inner width of individual pipettes was 600 μm while the inner height (the thick photoresist thickness) was 30 μm. The electroplated nickel walls were 20 μm thick. An example of a micromachined pipette array fabricated on top of a silicon substrate is shown in Figure 5.

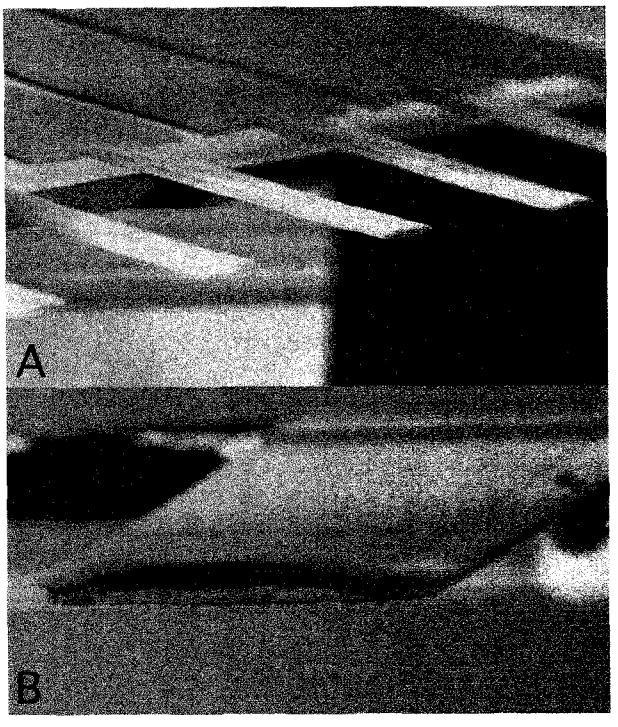

Figure 5. **A**. SEM micrograph of an array of pipettes extending from the silicon substrate. The wide sections are 12750×1500×30 μm^3 (L×W×H). Pipettes extend 1.5 mm from the substrate and are 500 μm wide. The structural material is electroformed nickel with wall thickness of 15 μm. **B**. Close-up of the end of a pipette. The inner cross-sectional area is 500×30 μm^2.

Interfaces machined from acrylic were used to interface the fabricated micromachined pipette arrays (MPA) with 397 μm inner diameter Teflon tubing. The acrylic interfaces were attached to the MPA via an ultra-violet (UV) curable adhesive. Teflon tubing connected the acrylic interfaces to either a pressure source or a pressure transducer. A photograph of an interfaced micromachined pipette array is shown in Figure 6.

The experimental data were obtained for water flows at room temperature with Reynolds numbers (*Re*) in the 1 to 100 range. The data indicate an increase in the friction factor (*f*), especially at the lower Reynolds number flows. The normalized friction coefficient, $C = (Re \cdot f)_{\text{exp.}} / (Re \cdot f)_{\text{theory}}$, was calculated to be approximately 1.45.

The experimental data and the Navier-Stokes and the general numerical model solutions are presented in Figure 7. The data are the average of three consecutive runs with bars indicating the data range. During each run, the syringe had to be refilled twice, resulting in three sets of data with slightly different slopes. In addition, at the higher flow rates, the compliance of the plastic syringe is believed to have resulted in actual flow rates slightly higher than those reported. Overall, the

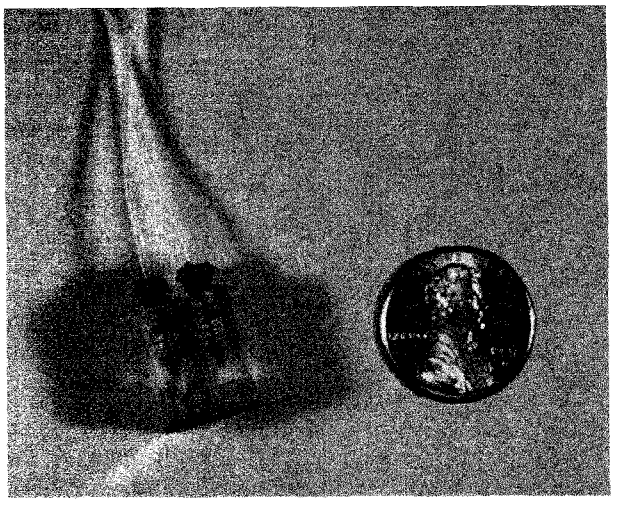

Figure 6. Photograph of a micromachined pipette array interfaced from the backside. Teflon tubing with a 397 μm inner diameter connects the acrylic interface to an external pressure source.

numerical model predicts the experimental data better than the classical Navier-Stokes theory.

The numerical model based on the micropolar fluid theory compares favorably with the currently available experimental data for volumetric flow rate as a function of driving potential (pressure difference) for water and blood in microchannels. Figure 8 shows our experimental data and data from Jiang et. al. [5] and Wilding et. al. [13] compared to values predicted by the numerical model. Channels used by Jiang were 10000×60×25.4 μm^3 (L×W×H), while channels used by Wilding were 11700×80×20 μm^3 (Figure 8, Wilding 1) and 11700×150×40 μm^3 (Figure 8, Wilding 2).

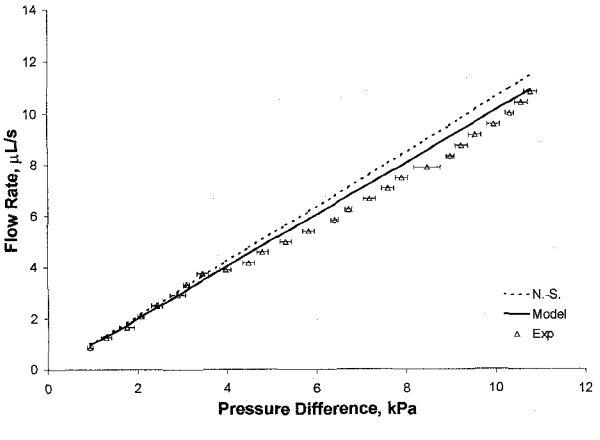

Figure 7. Comparison of experimental data, Navier-Stokes theory, and the numerical model for water flows in microchannels. Microchannels used to obtain experimental data were 3000×600×30 μm^3 (L×W×H).

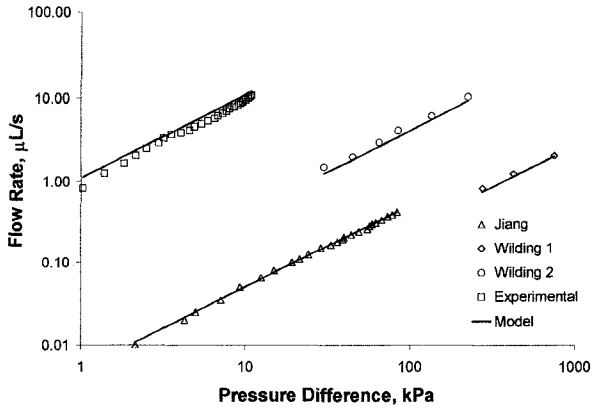

Figure 8. Comparison of experimental data with the model predictions for water flows in microchannels. Channels used by Jiang were 10000×60×25.4 μm^3 (L×W×H) [5], while channels used by Wilding were 11700×80×20 μm^3 (Wilding 1) and 11700×150×40 μm^3 (Wilding 2) [13]. Microchannels used to obtain experimental data were 3000×600×30 μm^3.

Microchannels used to obtain the new experimental data were 3000×600×30 μm^3. The numerical model provides a good prediction of experimental data over a wide range of channel sizes and flow rates.

CONCLUSION

Micromachining technologies have been used as a method of batch fabrication of metallic micromachined pipette arrays. These arrays were used to study fluid behavior on a micro-scale. A numerical model based on micropolar fluid theory provides a means of predicting flow characteristics, such as volumetric flow rate, average velocity, pressure drop, and friction factor for incompressible fluids operating in microchannels. The experimental results indicate a reduction of volumetric flow rate for a specified driving potential compared to macroscale predictions from the classical Navier-Stokes theory. The numerical model provides a better approximation of the experimental data than the Navier-Stokes theory. This information is essential to the successful design and development of future microfluidic devices.

ACKNOWLEDGEMENTS

The authors would like to acknowledge Hoechst, Inc. for supplying AZ4620 photoresist, James Stephenson for help with numerical analysis, Jack Cory of HEDCO Microelectronic Laboratory, Daniel Wright for help with acrylic interfaces, and the University of Utah Undergraduate Research Opportunity Program (UROP). This material is based upon work supported by a University of Utah Technology Innovation Grant.

REFERENCES

[1] S. C. Terry, J. Jerman, and J. Angell, *IEEE Trans. Electron. Devices,* Vol. ED-26, pp. 1880-6, 1979.

[2] E. Bassous, H. H. Taub, and L. Kuhn, *Appl. Phys. Lett.*, Vol. 31, pp. 135-7, 1977.

[3] R. W. Tjerkstra, M. de Boer, E. Berenschot, J. G. E. Gardeniers, A. van den Berg, and M. Elwenspoek, *Proc. MEMS 97*, Nagoya, Japan, Jan. 26-30, 1997.

[4] J. P. Brody and P. Yager, *Proc. Solid-State Sensor and Actuator Workshop*, Hilton Head, SC, June 2-6, pp. 105-108, 1996.

[5] X. N. Jiang, Z. Y. Zhou, J. Yao, Y. Li, and X. Y. Ye, *Proc. Transducers 95*, Stockholm, Sweden, June 25-29, pp. 317-320, 1995.

[6] X. F. Peng and B. X. Wang, *Proc. 10th International Heat Transfer Conference*, Brighton, UK, Aug. 14-18, pp. 159-177, 1994.

[7] D. B. Holmes and J. R. Vermeulen, *Chem. Engng. Sci.,* Vol. 23, pp. 717-722, 1968.

[8] J. N. Israelachvili, *J. Colloid Interface Sci.*, Vol. 110, pp. 263-271, 1986.

[9] M. L. Forcada and C. M. Mate, *J. Colloid Interface Sci.*, Vol. 169, pp. 218-225, 1993.

[10] P. Wu and W. A. Little, *Cryogenics*, May, pp. 273-277, 1983.

[11] J. Pfahler, J. Harley, H. Bau, and J. Zemel, *Proc. ASME*, DSC-Vol. 32, pp. 49-60, 1991.

[12] S. B. Choi, R. F. Barron, and R. O. Warrington, *Proc. ASME*, DSC-Vol. 32, pp. 123-134, 1991.

[13] P. Wilding, M. A. Shoffner, and L. J. Kircka., *Clin. Chem.*, Vol. 40, pp. 43-47, 1994.

[14] A. C. Eringen, *Int. J. Engng. Sci.*, Vol. 2, pp. 205-217, 1964.

[15] A. C. Eringen and E. S. Suhubi, *Int. J. Engng. Sci.*, Vol. 2, pp. 189-203, 1964.

[16] A. C. Eringen, *J. Math. Mech.*, Vol. 16, pp. 1-18, 1966.

[17] A. C. Eringen and K. Okada, *Int. J. Engng. Sci.*, Vol. 33, pp. 2297-2308, 1995.

[18] I. Papautsky, H. Swerdlow, and A. B. Frazier, *J. Microelectromech. Sys.*, in review.

[19] I. Papautsky, J. Brazzle, H. Swerdlow, and A. B. Frazier, *Proc. EMBS 97*, Chicago, IL, Oct. 30 - Nov. 2, pp. 2281-2284, 1997.